Surface & Coatings Technology 429 (2022) 127948

Contents lists available at ScienceDirect

Surface & Coatings Technology

journal homepage: www.elsevier.com/locate/surfcoat

A comparative study of the structure and corrosion resistance of ZnAl hydrotalcite conversion layers at different Al^{3+}/Zn^{2+} ratios on electrogalvanized steel

Thu Thuy Pham [a,b], Thuy Duong Nguyen [a], Anh Son Nguyen [a], Yoann Paint [c], Maurice Gonon [b], Thi Xuan Hang To [a,d], Marie-Georges Olivier [b,c,*]

[a] Institute for Tropical Technology, Vietnam Academy of Science and Technology, 18 Hoang Quoc Viet, Cau Giay, Hanoi, Viet Nam
[b] Université de Mons, Materials Science Department, Place du Parc 20, Mons, Belgium
[c] Materia Nova, Parc Initialis, Mons, Belgium
[d] University of Science and Technology of Hanoi, Vietnam Academy of Science and Technology, 18 Hoang Quoc Viet, Cau Giay, Hanoi, Viet Nam

ARTICLE INFO

Keywords:
Electrogalvanized steel
Hydrotalcite conversion coating
Corrosion resistance

ABSTRACT

The dissimilarities of the composition, crystal structure, and corrosion resistance of ZnAl hydrotalcite (ZnAl-HT) conversion films grown "in situ" on electrogalvanized (EG) steel substrate were investigated for different Al^{3+}/Zn^{2+} ratios at pH 12. The corrosion behavior of all conversion films in 0.1 M NaCl was compared through electrochemical techniques. The composition, morphology, structure, and thickness of conversion films with different Al^{3+}/Zn^{2+} ratios were characterized by Fourier-transform infrared spectroscopy (FT-IR), scanning electronic microscopy (SEM), and electron microscopy/energy dispersive X-ray spectroscopy (SEM/EDS), and X-ray diffraction (XRD). The polarization curves indicated that the ZnAl-HT films provided anodic inhibition for EG steel and the inhibition efficiency of the ZnAl-HT conversion films increases sharply with decreasing the Al^{3+}/Zn^{2+} ratios from 5/1 to 5/3, while, for the 5/4 and 5/5 ratios, the corrosion resistance of ZnAl-HT conversion films showed a downward trend after two immersion hours. However, the corrosion behavior of HT conversion films with the Al^{3+}/Zn^{2+} ratios from 5/3 to 5/5 remained stable for a longer immersion time. The protection performance of the ZnAl-HT films can be attributed to the barrier effects, ion-exchange competitive adsorption of chloride ions, and protective deposition of ZnO on the EG steel surface.

1. Introduction

Carbon steel with cost-effectiveness, easy processing, and high mechanical properties are predominantly used in large fields such as metallic structures, buildings, bridges, household appliances, transport sectors, and so on [1,2]. The main disadvantage of carbon steel is its poor corrosion resistance, which remains a major issue for ecological safety and economic development. In industries, the most common means for protecting steel against corrosion is cathodic protection. Among the different ways of cathodic protection, the zinc sacrificial layer is the most used for steel [3,4]. Nevertheless, unlike other active light metals as Ti and Al, zinc alloys cannot form a spontaneous passive oxide film for avoiding the substrate being exposed to corrosive environments [5]. So that, a lot of surface modification methods such as chemical conversion coatings [6–9], polymer coatings [10,11], and silane coatings [12,13], were developed for application on zinc and galvanized steel surfaces to block the penetration of the corrosive species to the substrates. Among these different protective films and coatings, hydrotalcites are more and more investigated [6–8].

Hydrotalcites (HTs) are anionic clays with a highly tunable brucite structure [14]. Although natural hydrotalcite was discovered in Sweden around 1842, this compound was firstly synthesized in the lab by Feitknecht in the next 100 years [15,16]. They have a chemical formula of $[M_{1-x}^{2+}M_x^{3+}(OH)_2][A^{n-}]_{x/n}\cdot mH_2O$, where M^{2+} and M^{3+} represent divalent (e.g., Mg^{2+} Cu^{2+}, Mn^{2+}, Ni^{2+} or Zn^{2+}) and trivalent metallic cations (e.g., Al^{3+}, Cr^{3+}, Fe^{3+}, In^{3+}, Mn^{3+} or Ga^{3+}), respectively, and the A^{n-} exchangeable anions are intercalated in the interlayer region for charge balance [17,18]. Also, x indicates the molar ratio of $M^{3+}/(M^{2+}+M^{3+})$, its value ranges from 0.20 to 0.33, and m indicates the water content in the hydrotalcite interlayer [18]. Hydrotalcites have the merits

* Corresponding author at: Université de Mons, Materials Science Department, Place du Parc 20, Mons, Belgium.
E-mail address: marjorie.olivier@umons.ac.be (M.-G. Olivier).

https://doi.org/10.1016/j.surfcoat.2021.127948
Received 15 October 2021; Received in revised form 19 November 2021; Accepted 22 November 2021
Available online 27 November 2021

Table 1
The conditions of treatment solutions used for the preparation of ZnAl-HT conversion films at room temperature with the different Al^{3+}/Zn^{2+} molar ratios on EG steel substrate.

No.	Sample	Concentration (M)		Time of the aging solution (h)	Synthesis time (h)	pH
		Al $(NO_3)_3$	Zn $(NO_3)_2$			
1	HT 5/1	0.05	0.01	6	16	12.0
2	HT 5/2	0.05	0.02	6	16	12.0
3	HT 5/3	0.05	0.03	6	16	12.0
4	HT 5/4	0.05	0.04	6	16	12.0
5	HT 5/5	0.05	0.05	6	16	12.0

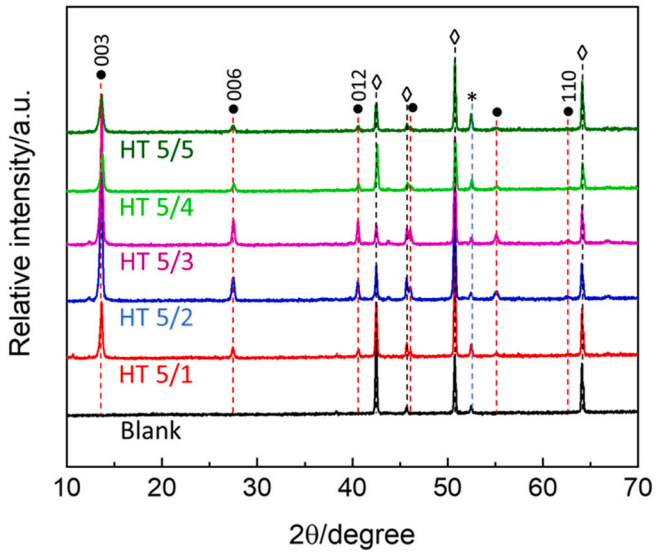

Fig. 1. XRD patterns of the EG steel substrate and the ZnAl-HT conversion films with the different Al^{3+}/Zn^{2+} molar ratios. Peaks marked with ● are contributed to ZnAl-HT, ◊ and * are due to Zn and Fe, respectively.

Table 2
The indexing of XRD for the ZnAl-HT conversion films with different Al^{3+}/Zn^{2+} molar ratios on EG steel substrate.

Parameter (nm)	HT 5/1	HT 5/2	HT 5/3	HT 5/4	HT 5/5
d(003)	0.760	0.761	0.760	0.762	0.760
d(006)	0.378	0.379	0.378	0.379	0.379
d(110)	0.173	0.173	0.172	0.172	0.172
Lattice parameter a	0.345	0.345	0.344	0.344	0.344
Lattice parameter c	2.279	2.282	2.279	2.285	2.280
Crystallite size d	29.504	42.983	34.672	40.080	35.846
(003)/(006) peak height ratio	5.743	5.291	5.433	4.729	4.522

of diversity in compositions, novel structure, and exceptional anion-exchangeability [19]. Hydrotalcites with anion exchange capacity are used as inhibitor containers for protection against corrosion of metals and alloys [20,21]. Moreover, they can directly grow on metal substrates and form a protective film with strong adhesion by simple synthesis methods. [17,22]. Recently, the "in situ" method has been investigated for the fabrication of the conversion films on metal substrates.

Uan et al. were the first to prepare MgAl-HT films on AZ91 Mg alloy by an "in situ" growth technique in HCO_3^-/CO_3^{2-} solution at different times and pH values [23–25]. After 72 h of salts spray test, they did not observe obvious corrosion on Mg substrates with treatment. Zhang et al. fabricated MgAl-HT films on the AA5005 aluminum alloy by hydrothermal treatment at various reaction times and pH solutions [26]. They showed that prolonging the crystallization time improved the

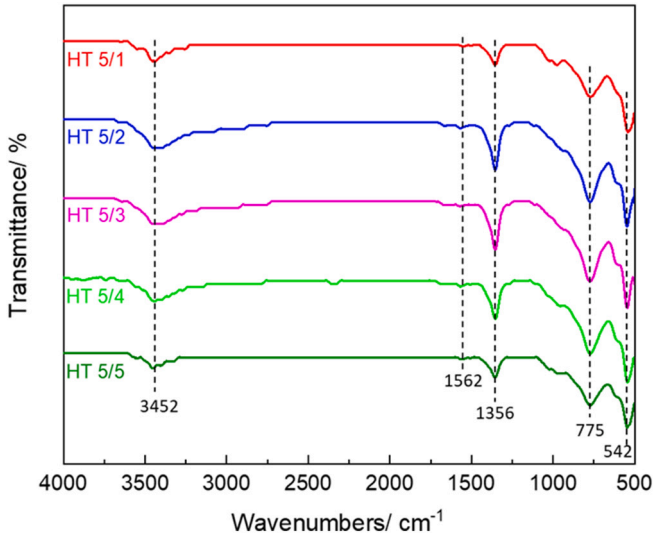

Fig. 2. FT-IR spectrum of the ZnAl-HT conversion films with the different Al^{3+}/Zn^{2+} ratios.

deposition, the protection performance of the obtained MgAl-HT films, and the optimum pH solution was 10. In alkaline solution, the zinc alloys can provide the Zn^{2+} cations, so the HT conversion films have already been grown "in situ" on zinc and galvanized steel substrates [6–8]. Buchheit et al. [6] firstly prepared carbonate intercalated ZnAl-HT films on hot-dip galvanized steel by dipping the substrate in a high alkaline sodium aluminate solution. Later, Hoshino et al. [7,8] also used this method to synthesize ZnAl-CO_3 HT films on EG steel and investigated the effect of the solution pH on HT films formation. They indicated that the solution pH affected the thickness, microstructure, compositions, and protective properties of the ZnAl-HT conversion films. Besides, the ZnAl-NO_3 HT film was grown "in situ" on zinc substrate. The zinc substrates were dipped in a mixture of $Al(NO_3)_3$ and $NaNO_3$ solutions at pH 3.2 and 90 °C [27,28]. However, the appeared cracks on the HT films, and the heterogeneous ZnAl-NO_3 HT films reduced their protective properties.

Very recently, the process of hydrotalcite formation and anti-corrosion by the ZnAl-HT coatings on galvanized steel have been started to be investigated [6–8]. However, the optimal conditions for the preparation of ZnAl-HT conversion film on EG steel have not yet been fully characterized. The change of metal cation's size, the charge, and the ratios could lead to modification of charge and orientation of anions, and, the relative amount of intercalated water, which affect the crystal structure parameters of HTs, bond strength, and anion exchange capacity [29–31]. In addition, Asl et al. fabricated and characterized HT coatings with different M^{3+}/M^{2+} ratios on magnesium alloy [32]. They indicated that the M^{3+}/M^{2+} ratios affected the shape and the size of HT crystals, as well as the crystallinity and anti-corrosion of HT films.

Therefore, this work aims to study the role of the Al/Zn ratios in controlling the morphology, structure, and protection properties of the ZnAl-HT conversion films grown on EG steel. The ZnAl-CO_3 HT conversion coatings were performed on the EG steel substrates using the "in situ" method. The samples were immersed in mixture solutions of Al $(NO_3)_3$ and $Zn(NO_3)_2$ at pH 12. The obtained ZnAl-HT conversion films were characterized using XRD, FT-IR, SEM, and EDS. The protection performance of all ZnAl-HT films was evaluated by electrochemical methods. The action mechanisms of these HT films were also discussed.

2. Experimental method

2.1. Materials

The studied substrate was electrogalvanized (EG) steel. The AISI

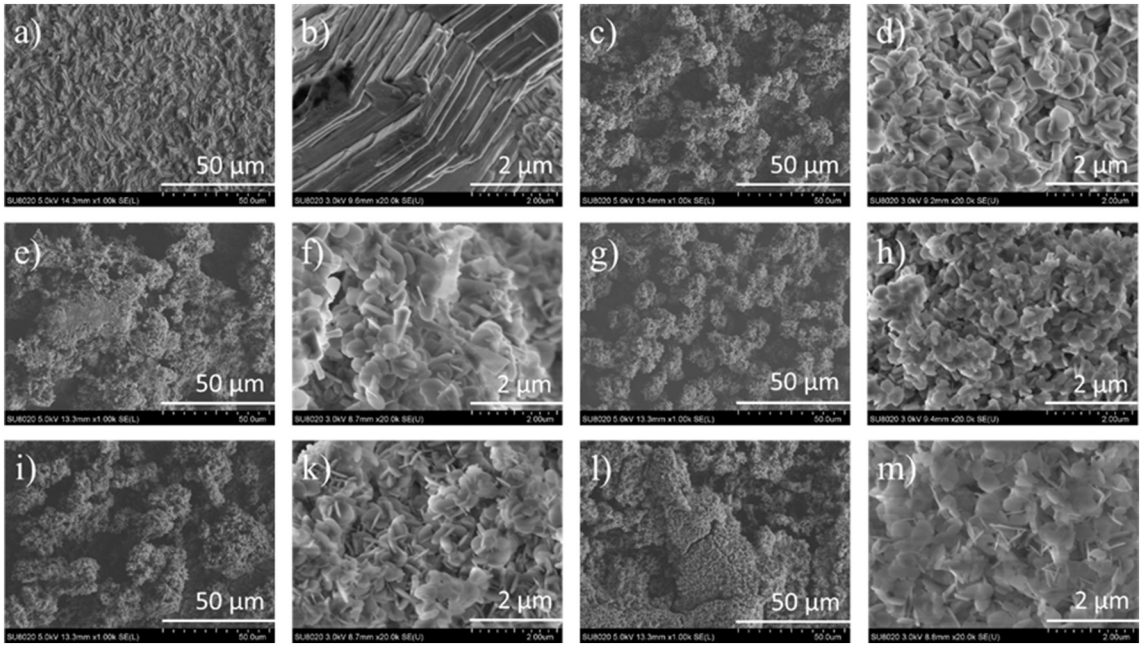

Fig. 3. SEM images of the EG steel substrate (a, b) and the ZnAl-HT conversion films with the different Al^{3+}/Zn^{2+} ratios 5/1: (c, d), 5/2 (e, f), 5/3 (g, h), 5/4 (i, k), and 5/5 (l, m).

Table 3
Element contents obtained from the EDS results of the original substrate and HT conversion films with the different Al^{3+}/Zn^{2+} ratios.

Sample	Element content (wt%)				Atomic ratio Al/Zn
	Zn	Al	O	C	
Blank	97.1	–	1.8	1.1	–
HT 5/1	46.7	9.8	41.6	1.9	0.51
HT 5/2	44.0	13.5	41.2	1.3	0.75
HT 5/3	45.6	10.6	42.5	1.4	0.56
HT 5/4	47.2	9.4	42.1	1.3	0.48
HT 5/5	50.5	8.7	39.5	1.3	0.42

4337 steel samples (25 × 32 × 2 mm) were cleaned by dipping in ATF SYSTOCLEAN 507 solution at current density (cathodic) of 30 $mA{\cdot}cm^{-2}$ for 3 min, rinsed with deionized water, and immersed in a mixture H_2SO_4/HCl 10% solution for 1 min before zinc electroplating. Two Pt-coated titanium counter electrodes were used for the electrodeposition process. The zinc electroplating was carried out in a bath containing 221.42 g $ZnSO_4{\cdot}7H_2O$ dissolved in 1000 mL deionized water. The pH of the solution was adjusted and maintained at 2 by adding 0.1 M H_2SO_4. The electrolysis was conducted at a direct current density of 50 $mA{\cdot}cm^{-2}$ at 40 °C for 11 min. The cross-sectional microstructure analysis of the specimens was carried out using Hitachi SU8020 FE-SEM. The layer was composed of pure zinc with a thickness of 8.50 µm. Before the synthesis experiment, the substrates were cleaned using a commercial alkaline solution Gardoclean (10 g/L) for 30 s, further washed several times with deionized water, and dried in cool air. The roughness of the zinc deposit was determined by optical profilometry using NanoJura device. Three measurements were performed on a 4 mm length scanned with 100 µm/min. The R_a value of the bare electrocoated sample was 1.3 ± 0.2 µm.

Aluminum nitrate nonahydrate $Al(NO_3)_3{\cdot}9H_2O$ was purchased from Sigma Aldrich and zinc nitrate hexahydrate $Zn(NO_3)_2{\cdot}7H_2O$ was purchased from Fluka, while ethanol, sodium chloride, and sodium hydroxide were supplied by VWR.

2.2. Experimental details

The ZnAl-HT films were prepared by the "in situ" growth method on the prepared EG steel substrate. In the typical synthesis, 0.05 mol Al $(NO_3)_3$ and 0.2 mol NaOH were dissolved in 1000 mL degassed distilled water and stirred for 15 min to form a homogeneous solution. $Zn(NO_3)_2$ was added to this mixture solution in a concentration range from 0.01 to 0.05 M (Table 1). The pH of the mixed solution was adjusted at 12 by the addition of 1 M NaOH solution as needed. The test specimens were immersed in the prepared solutions and stirred for 6 h, after which these substrates were kept in immersion in the selected solutions without stirring for 16 h. The synthesis was performed at room temperature. After the reaction, the substrates were rinsed several times with deionized water, ethanol and dried at 70 °C for 2 h in an oven.

The cross-section of all samples was prepared by sample epoxy embedding (Epoxy fix resin supplied by Stuers). Before characterization, the surfaces of samples were ground with 400, 800, 1200, 2000, and 4000 SiC papers, respectively, and cleaned with water and ethanol before drying with cold air.

2.3. Characterization and electrochemical measurements

2.3.1. Characterization techniques

The crystalline structure of ZnAl-HT films was investigated by X-ray diffraction (XRD, Bruker D5000) with CoKα radiation (λ = 0.1789 nm) and Fe filter with a step of 0.02° and a scanning rate of 1°/min in the 2θ range from 10° to 70°.

The obtained ZnAl-HT films were characterized by Fourier-transform infrared spectroscopy (Bruker IFS 66 *v*/S) in ATR working mode, in the wavenumber range from 500 to 4000 cm^{-1} at room temperature.

The morphology, thickness, and elemental composition of ZnAl-HT conversion films were determined via a field emission scanning electronic microscope (FE-SEM, Hitachi SU8020) with an energy dispersive X-ray spectrometer analyzer (EDS, Thermo Scientific Noran System 7).

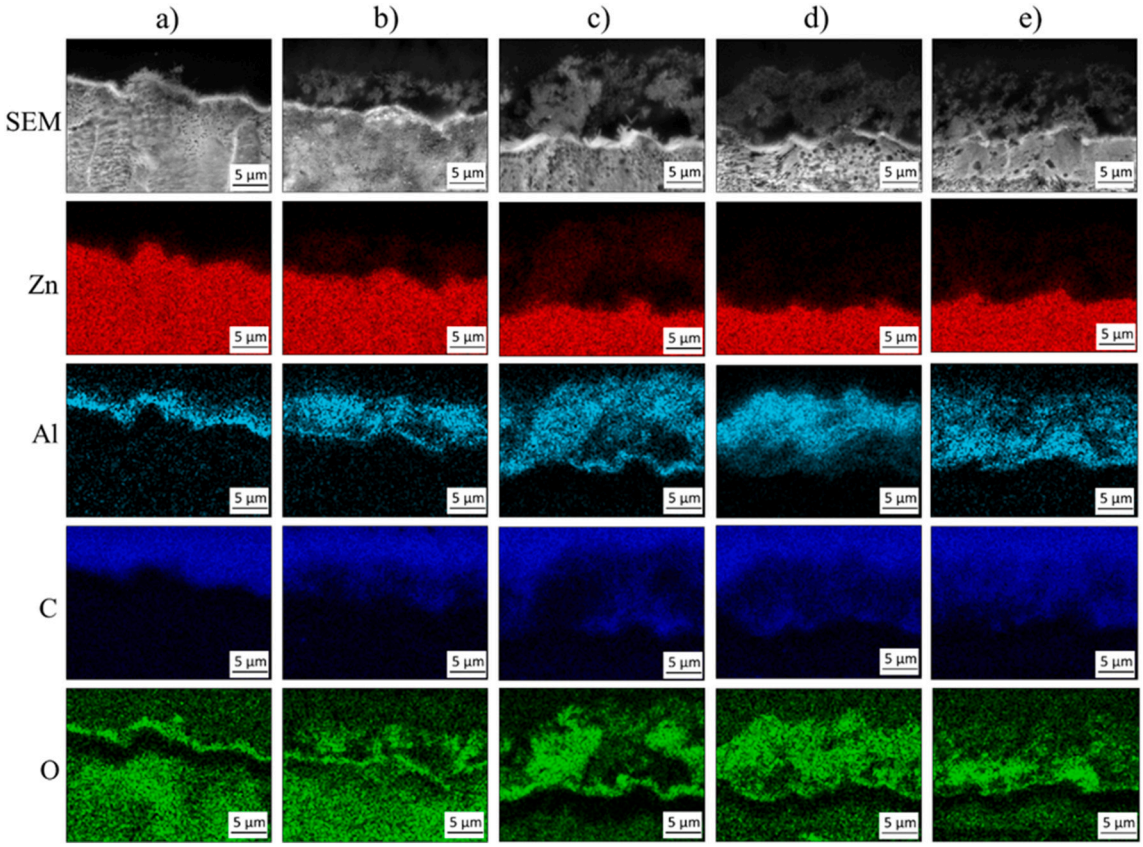

Fig. 4. SEM and EDS maps of the cross-sections of the ZnAl-HT conversion films for the different Al^{3+}/Zn^{2+} molar ratios: 5/1 (a), 5/2 (b), 5/3 (c), 5/4 (d), and 5/5 (e).

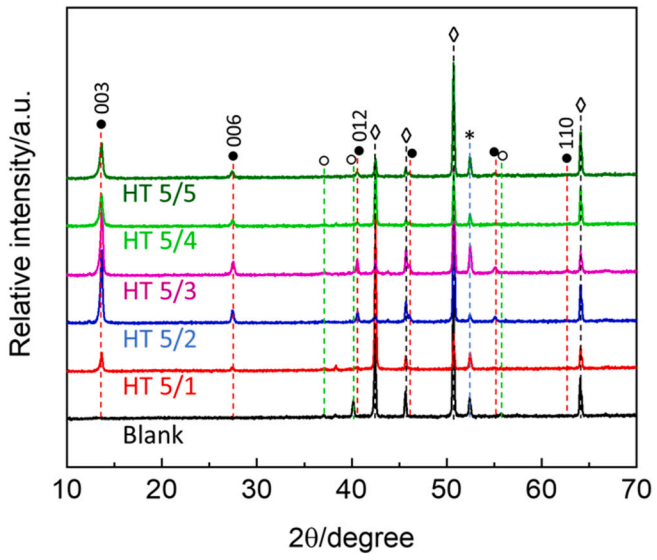

Fig. 5. XRD patterns of the EG steel substrate and the ZnAl-HT pretreated EG steel samples for the different Al^{3+}/Zn^{2+} ratios after immersion in 0.1 M NaCl for 24 h. Peaks marked with ● are related to the ZnAl-HT, ○ are attributed to ZnO, ◊ and * are due to the Zn and Fe, respectively.

2.3.2. Electrochemical measurements

The electrochemical measurements were performed in 0.1 M NaCl solution using a Parstat Model 2273 controlled by Powersuite® software. A classical three-electrode system, which consisted of a large platinum counter electrode, an Ag/AgCl (sat. KCl) reference electrode, and electrogalvanized steel samples as working electrodes with an exposed area of 1 cm^2 was used. The electrolyte was a solution of 0.1 M NaCl. EIS spectra were determined in a frequency range from 100 kHz to 10 mHz with 50 points using a 5 mV peak-to-peak sinusoidal voltage by Parstat 2273. Each experiment was done at least three times. Potentiodynamic polarization curves were carried out after 24 h of exposure in 0.1 M NaCl. The sweep rate was 0.2 mV s^{-1}. The scan was performed starting from 30 mV below OCP in the anodic direction.

3. Results and discussion

3.1. Structure, morphology, and elemental analysis of the ZnAl-HT conversion films with different Al^{3+}/Zn^{2+} ratios

Fig. 1 shows the XRD spectra of the ZnAl-HT conversion films developed on the EG steel substrate for the Al^{3+}/Zn^{2+} molar ratios ranging from 5/1 to 5/5. Four dominant peaks from the zinc layer were located at 42.48°, 45.72°, 50.76°, and 64.08°, which correspond to Zn (101), Zn(102), Zn(103), and Zn(110) planes, respectively (JCPDS No. 00-004-0831). The peak around 52.44° corresponds to Fe coming from the EG steel substrate (JCPDS No. 00-006-0696). Besides the peaks from the etched EG steel substrate, spectra of ZnAl-HT conversion films presented other characteristic peaks of hydrotalcites. The identical peaks at around 13.60°, 27.30°, and 40.50° corresponding to the (003), (006), and (012) reflections were characteristic of the layered structure of hydrotalcite. This indicates that the prepared HT films presented the expected crystallinity. The patterns displayed evidence of the unique presence of $Zn_6Al_{12}(OH)_{16}(CO_3^{2-})\cdot 4H_2O$ HT (JCPDS No. 00-038-0486). In the reaction forming HT coating, CO_3^{2-} anion can be provided from the air [7,8].

$$CO_2(g) + 2OH^- \rightarrow CO_3^{2-} + H_2O \quad (1)$$

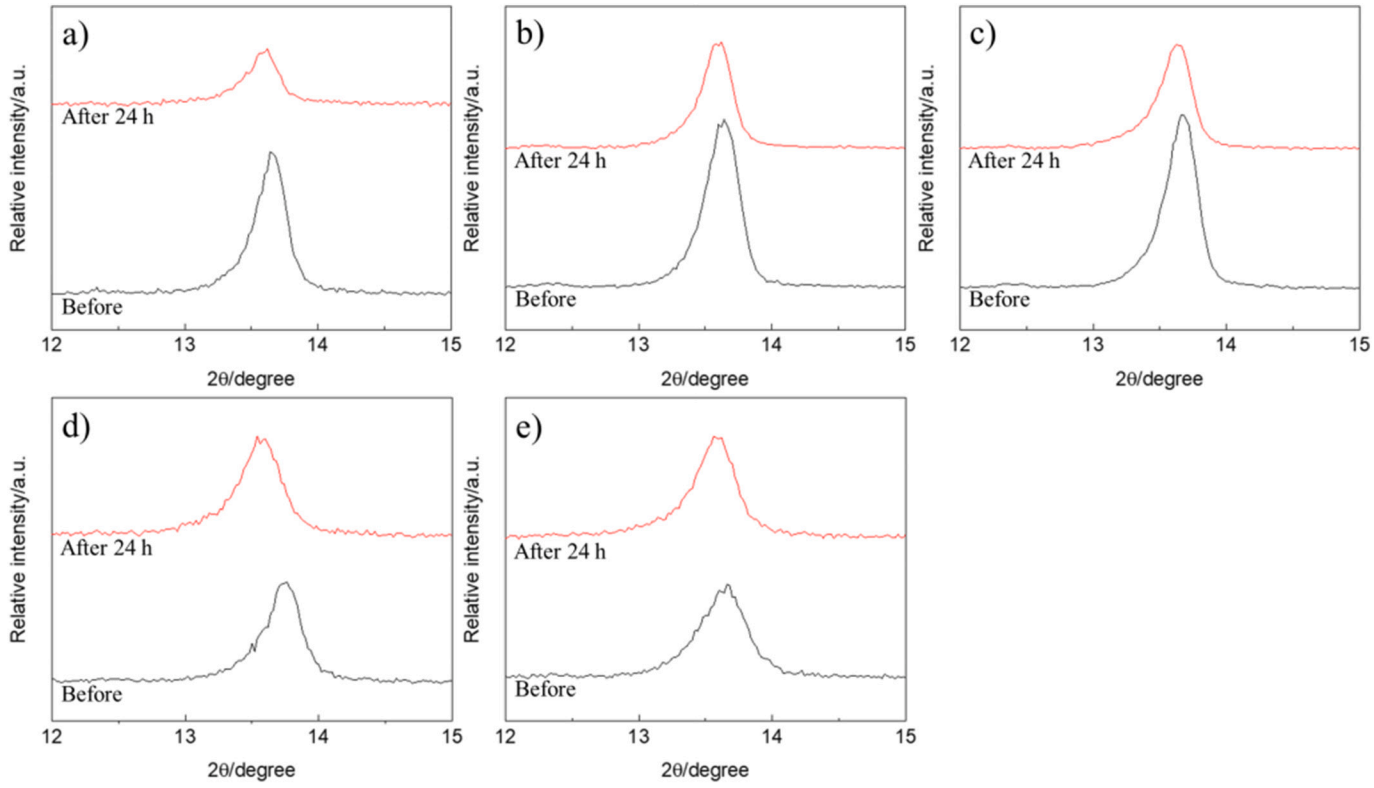

Fig. 6. XRD patterns of the ZnAl-HT pretreated EG steel samples for the different Al^{3+}/Zn^{2+} ratios as 5/1 (a), 5/2 (b), 5/3 (c), 5/4 (d), and 5/5 (e) before and after immersion in 0.1 M NaCl for 24 h (the XRD detail from 12° to 15°).

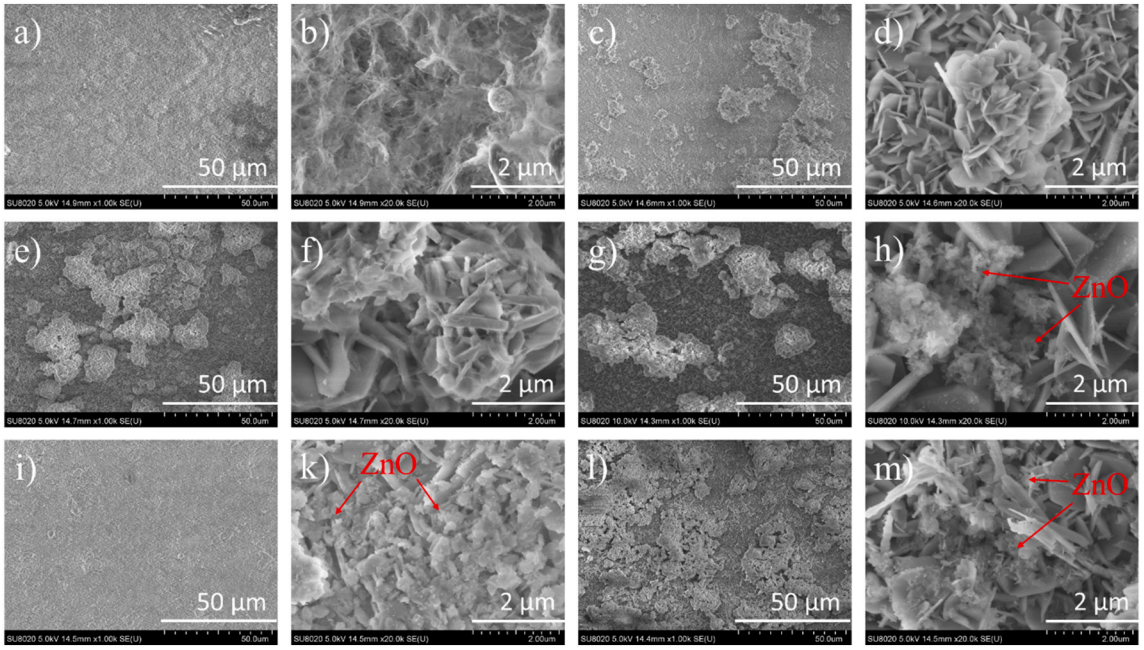

Fig. 7. SEM images of the EG steel substrate (a, b) and the ZnAl-HT pretreated EG steel samples for the different Al^{3+}/Zn^{2+} molar ratios as 5/1 (c, d), 5/2 (e, f), 5/3 (g, h), 5/4 (i, k), and 5/5 (l, m) after 24 h of immersion in 0.1 M NaCl.

The Zn^{2+} cations could be provided from the Zn metallic coating. The dissolved Zn^{2+} cations were added to the aqueous $Zn(NO_3)_2$ salt in the treatment solution and the dissolution reaction of Zn consisted of two reactions at the high end of the pH range [8]:

$$Zn(s) + 2OH^- \rightarrow ZnO(s) + H_2O + 2e^- \quad (2)$$

$$ZnO(s) + H_2O + OH^- \rightarrow Zn(OH)_3^- \quad (3)$$

Therefore, it is reasonable to assume that the following chemical reactions could occur at pH 12, resulting in the deposition of ZnAl-CO_3^{2-} HT films on the EG steel substrate.

$$12Al(OH)_4^- + 6Zn(OH)_3^- + CO_3^{2-} + xH_2O \rightarrow Zn_6Al_{12}(OH)_6(CO_3)\cdot 4H_2O + xOH^- \quad (4)$$

The lattice parameters (a, c) and the size of ZnAl-HT crystallites were determined from XRD patterns and presented in Table 2. The lattice parameter a corresponds to the brucite-like layer and the cation-cation distance and is calculated by the equation a = 2 × d(110). The lattice c parameter corresponding to the thickness of the interlayer distance is estimated by the equation c = 3 × d(003) [33,34]. The crystallite size of HTs can be obtained by applying the Scherrer equation at the strong characteristic peak (3):

$$d = \frac{0.9 \times \lambda}{FWHM \times \cos\theta}$$

where λ = 0.1789 nm is the wavelength of X-rays (Co K0α_1), FWHM is the full width at half maximum in radians, and θ is the diffraction angle for (003).

The basal spacing distances of HTs included the thickness of the brucite-like layer and the interlayer height, so the interlayer height can be derived by the equation: the interlayer height = d(003) – a [17,35]. The thickness of the brucite layer was around 0.345 nm, so the interlayer height was approximately 0.415 nm, the interlayer height was larger than the diameter of CO_3^{2-} anion (about 0.356 nm), it may due to the arrangement of carbonate anions between the layers [17,36]. The calculation results indicated that the c values of all samples did not reveal significant change as the Al^{3+}/Zn^{2+} molar ratio decreased, while the crystallite size tended to increase significantly from 5/1 to 5/2 and

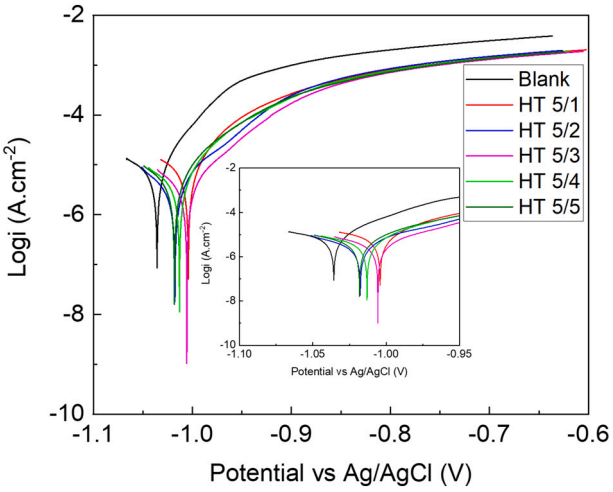

Fig. 9. Potentiodynamic polarization curves in 0.1 M NaCl of the bare EG steel substrate and the ZnAl-HT pretreated EG steel substrate samples for the different Al^{3+}/Zn^{2+} molar ratios.

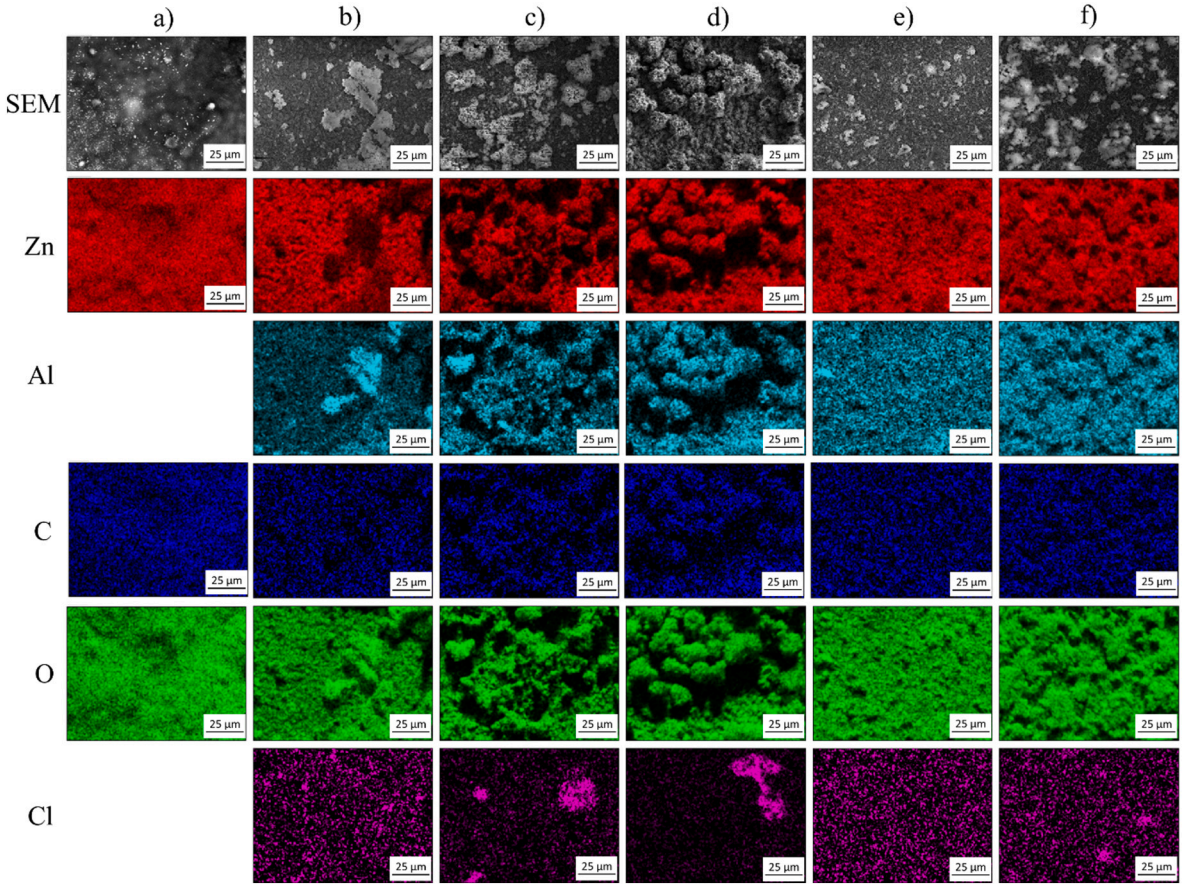

Fig. 8. EDS maps of the surface of bare substrate (a) and ZnAl-HT conversion films for the different Al^{3+}/Zn^{2+} ratios as 5/1 (b), 5/2 (c), 5/3 (d), 5/4 (e) and 5/5 (f) after immersion in 0.1 M NaCl for 24 h.

Table 4
Corrosion potential (E_{corr}) and corrosion current densities (i_{corr}) derived from the polarization measurement of the bare substrate and HT conversion films with the different Al^{3+}/Zn^{2+} ratios.

Sample	E_{corr} (V/Ag/AgCl)	i_{corr} ($A{\cdot}cm^{-2}$)
Blank	−1.04	2.63×10^{-6}
HT 5/1	−1.00	1.64×10^{-6}
HT 5/2	−1.02	0.72×10^{-6}
HT 5/3	−1.01	0.57×10^{-6}
HT 5/4	−1.01	0.54×10^{-6}
HT 5/5	−1.02	0.65×10^{-6}

did not change much with the other three ratios (Table 2). Moreover, the increase of the XRD intensity of the ZnAl-HT peaks was observed as the Al^{3+}/Zn^{2+} molar ratio decreased from 5/1 to 5/3, however, these characteristic peaks decreased at other 5/4 and 5/5 molar ratios. The large difference in cationic radii of Zn^{2+} (0.74 nm) and Al^{3+} (0.51 nm) could distort the hydroxide layers networks of the HT crystal, therefore, the decrease of Al^{3+}/Zn^{2+} ratios from 5/3 to 5/5 reduced the crystallinity of HT [37–39].

Moreover, the ZnAl-HT conversion films were also studied by FT-IR spectrum (Fig. 2). In the FT-IR spectrum of ZnAl-HT films, the absorption band at around 3450 cm^{-1} corresponded to the stretching vibration of the hydroxyl groups of hydrotalcite layers and crystal water in the interlayer region. Besides, the absorption band of about 1600 cm^{-1} can be assigned to the bending vibration of the intercalated crystal water [17]. The strong peak at 1356 cm^{-1} can be related to the characteristic band of asymmetric stretching vibration of the C—O in carbonate anion present in hydrotalcite [8]. In addition, the peaks at around 770 cm^{-1} and 540 cm^{-1} were attributed to the Al—O and Zn—O vibration modes.

The surfaces of all ZnAl-CO_3^{2-} HT films highlighted the nano-hexagonal plate morphology after treatment at all Al^{3+}/Zn^{2+} ratios, which confirmed that the HT films were formed and almost entirely covered the substrate (Fig. 3). The inclined growth of ZnAl-HT films nanoplates at the Al^{3+}/Zn^{2+} ratios were decreased from 5/1 to 5/3 as observed (Fig. 3d, f, h), while the nanoplates of ZnAl-HT conversion films at the ratios 5/4 and 5/5 presented an interlaced structure (Fig. 3k, m). Besides, the crystal size of the ZnAl-HT films tended to increase slightly as the Al^{3+}/Zn^{2+} ratios were decreased from 5/1 to 5/2, but at the Al^{3+}/Zn^{2+} ratio of 5/3, the crystals showed a marked size reduction and became more uniform and denser, which was effective for avoiding the substrate to be exposed to an aggressive environment. The crystals of ZnAl-HT films showed an upward trend in size and a downward trend in thickness when the Al^{3+}/Zn^{2+} molar ratios were decreased from 5/4 to 5/5. These changes of ZnAl-HT film's crystals at the Al^{3+}/Zn^{2+} ratios: 5/4 and 5/5 may be detrimental for anticorrosion properties. The EDS results showed that the ZnAl-HT films were almost composed of Zn, Al, O, and C elements (Table 3). Because the Zn content of all HT samples was derived from HT film and the Zn coating of the substrate, the Zn content did not change too much when reducing the Al^{3+}/Zn^{2+} ratios. The Al content was only contributed from HT films. When the Al^{3+}/Zn^{2+} ratios decreased from 5/1 to 5/2, the Al content on the surface increased from 9.8% to 13.5%. This means that the amount and the thickness of HT 5/2 film formed on EG steel substrate were larger than that of HT 5/1 film. This result was in good agreement with the SEM cross-sections (Fig. 4a, b). The increase of the Zn^{2+} concentration from 0.03 to 0.05 M did not affect the thickness of HT films (Fig. 4c-e), but it affected the atomic ratio Al/Zn (Table 3). The decrease of the atomic ratio Al/Zn

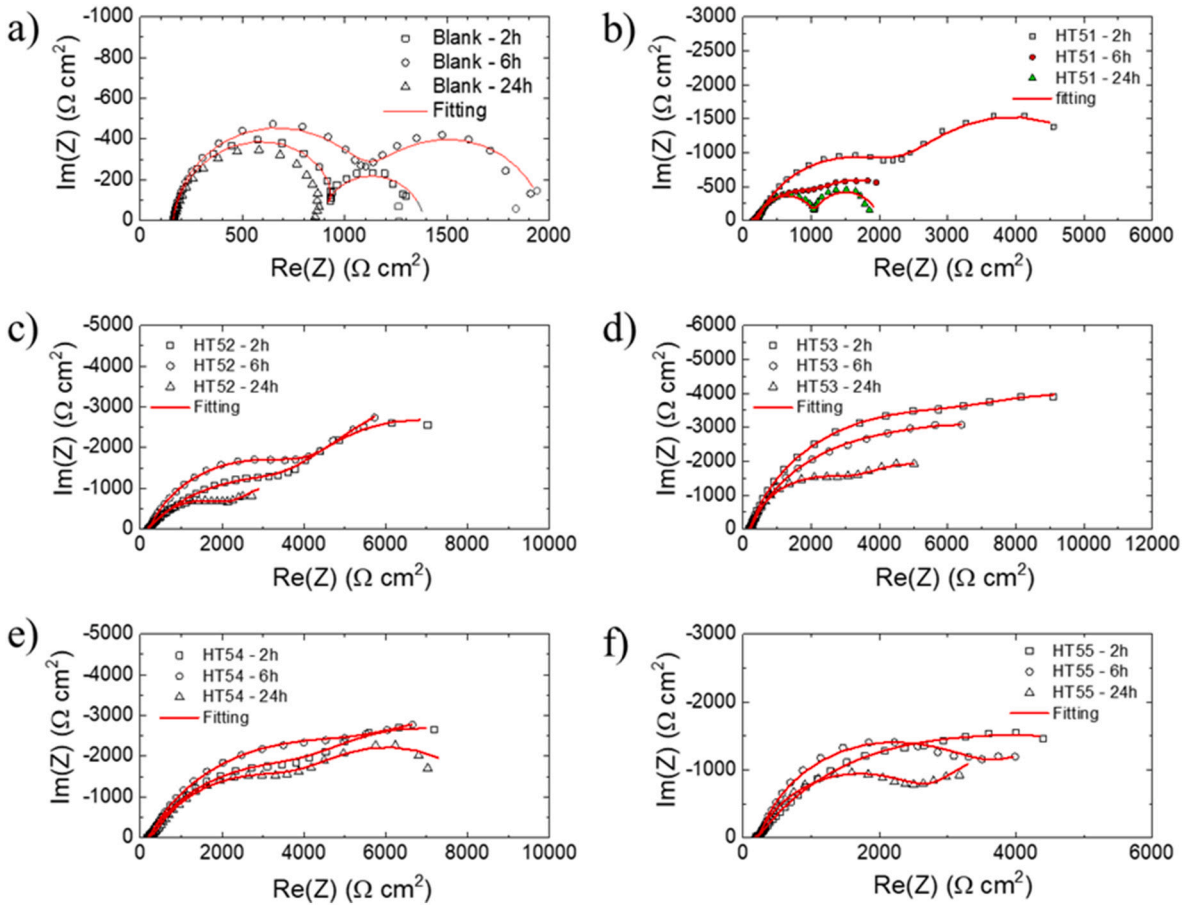

Fig. 10. Nyquist plots of the bare substrate (a) and the ZnAl-HT conversion films with different Al/Zn ratios as 5/1 (b), 5/2 (c), 5/3 (d), 5/4 (e), and 5/5 (f) immersion in 0.1 NaCl for 2 h, 6 h, and 24 h.

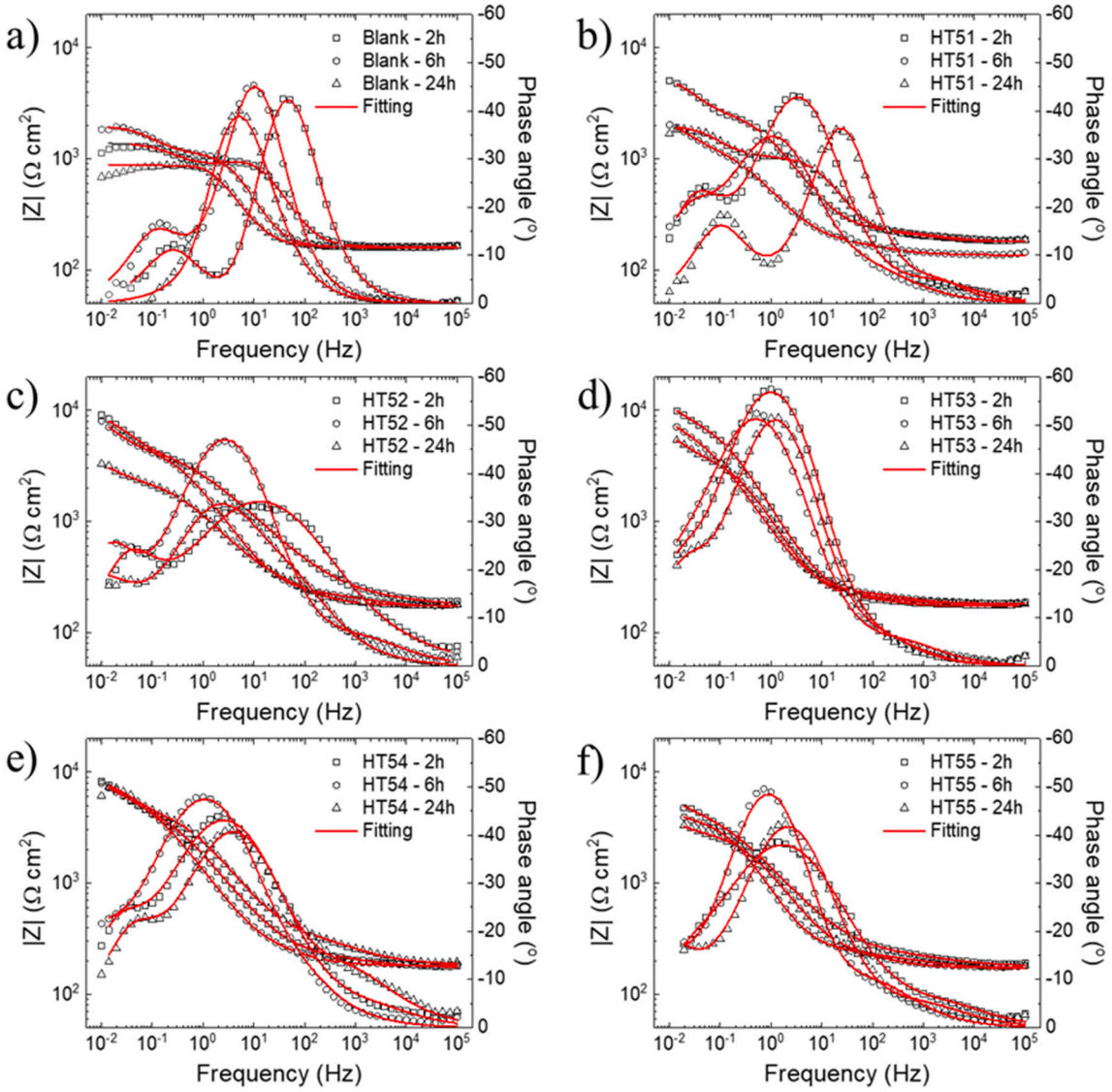

Fig. 11. Bode plots of the bare substrate (a) and the ZnAl-HT conversion films with different Al/Zn ratios as 5/1 (b), 5/2 (c), 5/3 (d), 5/4 (e), and 5/5 (f) immersion in 0.1 NaCl for 2 h, 6 h, and 24 h.

indicated that the change of Al^{3+}/Zn^{2+} ratios affected the composition of HT films [38].

Fig. 4 presents the cross-sections and EDS maps of all ZnAl-HT conversion film samples embedded in resin. Elemental maps of Al, Zn, C, and O revealed the elemental distribution on the surface of HT films. Therefore, it can be easily deduced that the ZnAl-HT conversion films were grown on an EG steel substrate. The change of Al^{3+}/Zn^{2+} tended to lead to a change in the dissolution rate of zinc from the top coating substrate, the porosity, and the thickness of the HT films. The thicknesses of the HT films measured via cross-sectional SEM images were around 1.1, 5.2, 14.3, 14.0, and 14.0 μm for the HT 5/1, 5/2, 5/3, 5/4, and 5/5 Al^{3+}/Zn^{2+} ratios, respectively. The thickness of HT conversion films increased significantly with the decrease of the Al^{3+}/Zn^{2+} molar ratio down to 5/3 and the stability of conversion films thickness was observed at the remaining ratios. Some gaps which appeared in the cross-section of HT films were observed from SEM surface morphology images at lower magnifications (Fig. 3). It appears that the porosity of the HT 5/3 and HT 5/4 conversion films was higher than those of the other three samples, which coincided with the obtained results from SEM images of the sample surfaces (Fig. 3).

The variation of the concentration in Zn^{2+} in solution did not significantly affect the structure of the ZnAl-HT films. Nevertheless, the variation of the Zn^{2+} concentration can modify the dissolution reaction of the zinc layer, the conversion film's thickness, and its porosity. When the zinc ions were provided by the solution, the thickness of the HT layer was increased but an optimal value was required to lead to a more uniform and compact layer.

3.2. *Characteristics of the ZnAl-HT conversion films with different Al^{3+}/Zn^{2+} ratios after immersion in 0.1 M NaCl for 24 h*

The XRD patterns of the bare substrate and the ZnAl-HT pretreated EG steel samples for the different Al^{3+}/Zn^{2+} molar ratios after immersion in 0.1 M NaCl for 24 h are shown in Fig. 5. Compared with the bare substrate, ZnO peaks appeared on the immersed samples, in addition to those of the EG steel substrate (JCPDS No. 00-036-1451). The XRD analysis revealed the ZnO crystalline phase, implying the occurrence of corrosion on the EG surface [40]. It is worth noting that the characteristic peaks of ZnAl-HT conversion films for the different Al^{3+}/Zn^{2+} molar ratios on EG steel substrate still existed after 24 h immersion test, but the intensity and sharpness of these ZnAl-HT peaks slightly decreased. The 2θ values of peaks corresponding to the (003) face of

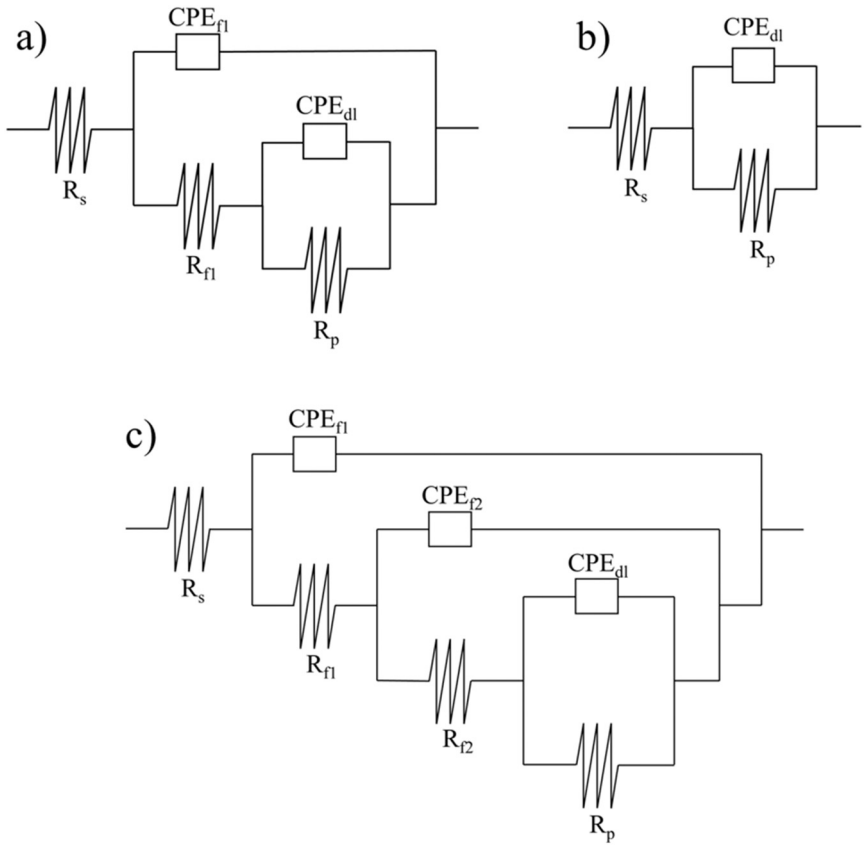

Fig. 12. Equivalent circuits used for fitting the electrochemical impedance diagrams.

Table 5
Results of fitting EIS diagrams and $|Z|_{10mHz}$ values for the bare substrate and HT films with the different Al^{3+}/Zn^{2+} ratios with immersion time.

Sample	R_s ($\Omega \cdot cm^2$)	CPE_{f1} ($\Omega^{-1} \cdot s^n \cdot cm^{-2}$)	n_{f1}	R_{f1} ($\Omega \cdot cm^2$)	CPE_{f2} ($\Omega^{-1} \cdot s^n \cdot cm^{-2}$)	n_{f2}	R_{f2} ($\Omega \cdot cm^2$)	CPE_{dl} ($\Omega^{-1} \cdot s^n \cdot cm^{-2}$)	n	R_p ($\Omega \cdot cm^2$)	$\|Z\|_{10\ mHz}$ ($\Omega \cdot cm^2$)
Blank-2h	162	1.49E-05	0.93	878	–	–	–	1.10E-03	0.9	896	1123
Blank-6h	161	5.30E-05	0.94	995	–	–	–	2.20E-03	0.9	821	1845
Blank-24h	160	–	–	–	–	–	–	1.47E-04	0.87	874	688
HT51-2h	180	3.11E-05	0.71	54	1.02E-04	0.79	2592	1.95E-03	0.9	2996	5031
HT51-6h	136	3.00E-04	0.64	83	2.96E-04	0.75	1316	6.92E-03	0.9	954	2031
HT51-24h	181	7.19E-06	0.88	44	2.30E-05	0.9	835	2.28E-03	0.9	933	1550
HT52-2h	176	4.67E-05	0.55	81	5.05E-05	0.52	5147	9.30E-04	0.9	5531	9021
HT52-6h	170	4.25E-05	0.66	72	8.37E-05	0.76	4990	1.96E-03	0.9	6727	8044
HT52-24h	174	1.02E-04	0.68	340	1.55E-04	0.67	2013	4.82E-03	0.77	2936	3308
HT53-2h	182	7.05E-05	0.79	52	1.04E-04	0.82	8681	1.92E-03	0.9	5588	10976
HT53-6h	182	6.71E-05	0.73	58	2.61E-04	0.76	7458	3.27E-03	0.9	3156	7832
HT53-24h	174	8.00E-05	0.8	61	1.40E-04	0.83	3883	2.83E-03	0.9	3258	5840
HT54-2h	174	3.74E-05	0.67	56	1.11E-04	0.66	5822	1.64E-03	0.9	4489	8291
HT54-6h	180	1.58E-04	0.68	304	5.91E-05	0.76	4053	3.61E-03	0.9	4487	7924
HT54-24h	185	3.78E-05	0.62	226	5.90E-05	0.72	4779	1.15E-03	0.9	3847	6108
HT55-2h	180	3.14E-05	0.65	62	1.97E-04	0.6	5239	4.18E-03	0.9	1219	4936
HT55-6h	172	1.21E-04	0.69	123	1.66E-04	0.86	3839	1.02E-02	0.9	2527	4408
HT55-24h	172	5.92E-05	0.66	60	1.43E-04	0.75	2862	7.50E-03	0.9	2649	3780

ZnAl-CO_3 HT (around 13.60°) decreased slightly after immersion in 0.1 M NaCl (Fig. 6). The recent researches indicated that the (003) reflection – d(003) corresponded to the basal spacing of 0.774 nm and 0.758 nm for ZnAl-Cl and ZnAl-CO_3 HT, respectively [41]. Besides, Iyi et al. demonstrated that the CO_3^{2-} ions in HT can be exchanged for Cl^- anions when immersed in NaCl solution [42]. Therefore, the increase in basal spacing and the decrease in sharp peaks of ZnAl-HT after immersion confirmed that Cl^- anions were intercalated and partially replaced the CO_3^{2-} anions in the interlayer region of hydrotalcite. This suggests that the as-prepared ZnAl-HT conversion films with the different Al^{3+}/Zn^{2+} ratios offered durable, protective properties and good corrosion resistance. Besides, the XRD pattern of the immersed HT-conversion film

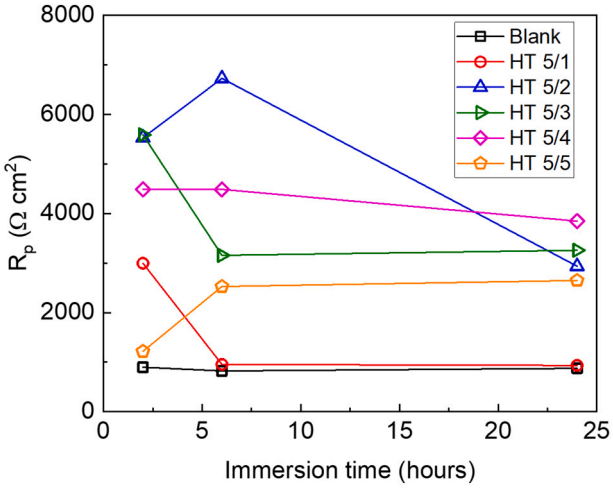

Fig. 13. Evolution of the values R_p of the ZnAl-HT conversion films with different Al/Zn ratios.

samples contained ZnO peaks with very low intensity, implying the occurrence of corrosion at the interface between these HT films and the EG steel substrate, and the retention in the solid phase of Zn^{2+} cations from the partial dissolution of hydrotalcites [43,44].

Fig. 7 shows the SEM morphologies of the EG steel substrate and the ZnAl-HT pretreated EG steel samples for the different Al^{3+}/Zn^{2+} ratios after 24 h of immersion in 0.1 M NaCl solution. All the ZnAl-HT conversion films on the EG steel substrate samples remained quite compact and intact with a platelet-like microstructure after immersion. However, compared with the original ZnAl-HT films, the morphologies after immersion presented several significant changes. The nano-plates of the HT 5/1 and HT 5/2 films with edges became slightly sharper after the immersion in the aggressive environment and a few crystals precipitated as flowers on the surface of these ZnAl-HT conversion films (Fig. 7b, c). The surfaces of HT 5/3 and HT 5/5 conversion films were partially covered by hexagonal crystals of ZnO due to the dissolution of the Zn from the substrate and ZnAl-HT films, while the ZnO precipitates were interweaved with the network of hydrotalcite crystals on the entire surface of the HT 5/4 conversion film. Moreover, the nano ZnO improved corrosion resistance by forming a thin layer on the metal surface [45], so the corrosion resistance of the HT 5/3, HT 5/4, and HT 5/5 remained stable during the surveyed period. In contrast, serious general corrosion occurred on the EG steel substrate without ZnAl-HT conversion films (Fig. 7a). The EDS analysis of all the ZnAL-HT conversion films after immersion in 0.1 M NaCl was presented in form of two-dimensional maps (Fig. 8). For the EG sample without HT film, the main components of the top layer included Zn, O, and C elements, which were relatively uniformly distributed. The presence of O with high intensity was noted on some zones, which were also enriched in Zn. This results indicated the formation of $ZnO/Zn(OH)_2$ on the surface of the bare substrate after 24 h. The EDS maps showed an uneven distribution of the Al, Zn, C, and O elements on almost all the ZnAl-HT conversion film samples, with an exception for that of the HT 5/4 sample, which proved that the surface of samples was highly uneven. Although the distribution of the required elements was uniform throughout the HT 5/4 film, these specific zones were enriched in both Zn and O. The main reason was that the intercalation of ZnO crystals in the HT structure blocked the gaps on the HT 5/4 film, which could also be verified in the XRD analysis. In addition, the presence of the element Cl was noted only on some specific zones, which was an indication of the absorption and retention of the aggressive Cl^- ions in HT interlayers.

3.3. Electrochemical test of the ZnAl-HT conversion films with different Al^{3+}/Zn^{2+} ratios

Fig. 9 presents the polarization curves of the bare Zn coated steel substrate and the ZnAl-HT pretreated EG steel samples after immersion in 0.1 M NaCl for 24 h. The determined corrosion potential (E_{corr}) and corrosion current densities (i_{corr}) were presented in Table 4. The corrosion potentials (E_{corr}) of the HT 5/1, HT 5/2, HT 5/3, HT 5/4, and HT 5/5 samples were around −1.00, −1.02, −1.01, −1.01, and −1.02 V, respectively, and were shifted toward more positive values compared to the blank EG substrate (−1.04 V). The i_{corr} value of the HT 5/1 (1.64×10^{-6} A·cm^{-2}) was only slightly lower than that of the blank substrate (2.63×10^{-6} A·cm^{-2}). A stronger decrease was determined for the four other samples (the i_{corr} values of HT 5/2, HT 5/3, HT 5/4, and HT 5/5 were 0.72×10^{-6}, 0.57×10^{-6}, 0.54×10^{-6}, and 0.65×10^{-6} A·cm^{-2}, respectively). Therefore, the ZnAl-HT films can be considered as anodic inhibitors for the EG steel substrate. The shift of E_{corr} to positive values and the decrease of the i_{corr} showed that the ZnAl-HT conversion films were protective and the corrosion resistance was gradually enhanced.

Besides the potentiodynamic polarization measurements, the electrochemical impedance diagrams (EIS) were determined in the same aggressive solution for the bare substrate and the ZnAl-HT pretreated EG steel samples for the different Al^{3+}/Zn^{2+} molar ratios. The EIS diagrams can give information such as film resistance and film capacitance, double layer capacitance, and charge transfer resistance [17]. Figs. 10 and 11 present Nyquist and Bode plots of samples immersed in 0.1 M NaCl for 2 h, 6 h, and 24 h.

For the bare substrate, the impedance diagrams exhibited two time constants after 2 h and 6 h immersion. The first time constant in the medium frequency region was related to the oxide film on the surface and the second one in the low frequency was related to the corrosion process [46]. Surface analysis by EDS indicated the deposition of a zinc oxide/hydroxide layer on the zinc surface during immersion time (Fig. 8a). The similar result was also reported [40]. The EIS diagrams for bare substrate immersed for 2 h and 6 h were fitted by the equivalent circuit of Fig. 12a and the fitting data were presented in Table 5. This circuit was composed of the solution resistance R_s, the resistance R_{f1}, and the constant phase element CPE_{f1} of the zinc oxide/hydroxide layer and, the resistance R_p and the constant phase element CPE_{dl} of the double layer. However, it was possible to observe one capacitive loop for bare substrate exposed for 24 h, presenting the beginning of localized corrosion and the merger of corrosion products into one layer [47]. This

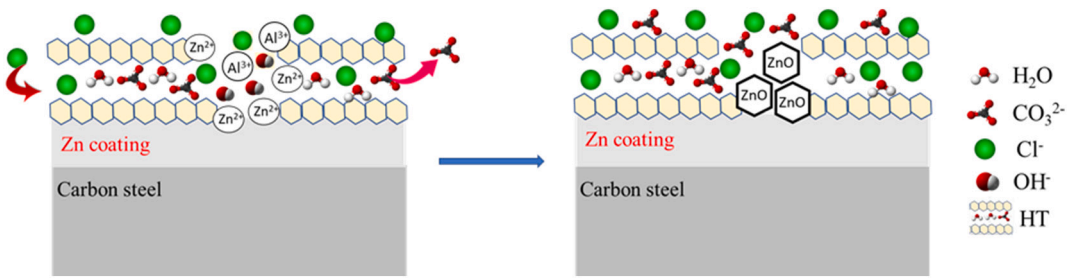

Fig. 14. The corrosion protection mechanism of the ZnAl-CO_3^{2-} HT conversion films.

result was completely consistent with the results of surface and structural analysis of the bare substrate after 24 h (Figs. 5 and 8a). The model $R_s(CPE_{dl}R_p)$ was used for the bare substrate after 24 h (Fig. 12b and Table 5). The quite high value of the calculated double layer capacitance can be attributed to the substrate roughness (1.3 ± 0.2 μm).

For all the HT conversion films, the three time constants were observed in the impedance diagrams during immersion time. The model $R_s(CPE_{f1}(R_{f1}(CPE_{f2}(R_{f2}(CPE_{dl}R_p)))))$ was used for fitting the EIS diagrams of all HT samples in the surveyed period (Fig. 12c) and the fitting parameters from impedance diagrams of electrodes were listed in Table 5. R_s, R_{f1}, R_{f2}, and R_p were the solution resistance, oxide film resistance, HT film resistance, and polarization resistance, respectively. CPE_{f1}, $CPE_{f2,}$ and CPE_{dl} presented the constant phase element of the oxide film, HT film, and double layer, respectively. From a general point of view, the system with the higher Z modulus at lower frequencies and the higher value of R_p exhibited higher corrosion resistance [17,20]. For the HT films with different Al^{3+}/Zn^{2+} ratios, the values of $|Z|_{10mHz}$ and R_p were largely higher than the ones of the blank sample (Fig. 11 and Table 5). This indicated that the anti-corrosion of the EG steel substrate was significantly improved with ZnAl-HT films.

For the HT 5/1 film, the Rp values decreased significantly from 2996 to 933 Ω·cm^2 with the increase of the immersion time. The values of R_p of HT 5/2 and HT 5/3 films after immersion for 2 h gained 5531 and 5588 Ω·cm^2, respectively, which were higher in comparison with the values obtained in HT 5/1 film. The significant enhancement in corrosion protection of the HT 5/2 and HT 5/3 films in comparison with the HT 5/1 conversion films after 2 h was attributed to the thickness increment of the HT films for this concentration range of Zn^{2+} cations in the synthesis solution (Fig. 4a-c). However, similar to HT 5/1 film, the R_p values of HT 5/2 and HT 5/3 films after 24 h also reduced sharply to 2936 and 3258 Ω·cm^2, respectively. This demonstrated that the low density of the HT 5/1, HT 5/2, and HT 5/3 conversion films facilitated the penetration of the aggressive species, the protection performance of these films did not remain stable after 24 h of exposure.

Regarding the fitting parameters obtained for the HT 5/4 and HT 5/5 films, the R_p values after 2 h was 4489 and 1219 Ω·cm^2, respectively, which showed a marked decrease compared to HT 5/3 sample (Fig. 13 and Table 5). This reduction could be explained as these crystals were thinner than that of HT 5/3 (Fig. 3g-m), so they were easily partially dissolved and the aggressive ions can easily penetrate. In contrast, these values remained stable after 24 h of immersion and the HT 5/4 reached the slightly higher final value after 24 h than the HT 5/3 one (Fig. 13 and Table 5). For the HT 5/5 sample, the R_p values were initially quite low after 2 h of immersion, but, their value doubled during the investigated period. This demonstrated that the protection performance of HT 5/5 film improved during immersion time. The intercalation of ZnO crystals in the HT structure blocked the gaps on the HT 5/4 and HT 5/5 that were observed from the SEM and XRD results (Figs. 5 and 7), which was the main reason for the improved corrosion resistance of these films.

In summary, the corrosion resistance of the EG steel substrate was significantly enhanced with HT films. The change of the Zn^{2+} cation concentration in the synthesis solution affected the crystal size, the thickness, and the density of the conversion films modifying their corrosion resistance. The optimum Al^{3+}/Zn^{2+} ratio seems to be around 5/3 and 5/4. To clarify this behavior, the samples were characterized after 24 h test in NaCl solution.

3.4. Corrosion protection mechanism of ZnAl-HT conversion film

From the experimental results, a corrosion protection mechanism model of the ZnAl HT conversion films on EG steel substrate was proposed in direct relation with the mechanisms of ion-exchange, deposition, and competitive adsorption (Fig. 14).

The density of ZnAl-HT films on EG steel substrate acted as a barrier layer against the chloride attack, however, they only protect substrate to a certain extent. During exposure to corrosive ions (Cl^-), the CO_3^{2-}anions intercalated between the metal cation layers of HT conversion films are partially exchanged with Cl^- anions. This ion exchange reaction, which was attributed to the absorption and retention of the aggressive Cl^- ions and the release of the CO_3^{2-} ions, was the main reason for reducing the aggressiveness of NaCl solution and improving the corrosion resistance of these films [48]. The recent published researches also proved that ZnAl-HT and MgAl-HT intercalated with carbonate anions were effective chlorides “nanotraps” due to the ion exchange process, so the HT films could delay the substrate degradation [48,49]. The ion exchange reaction of ZnAl-HT conversion film on EG steel substrate in chloride containing solution can be expressed as follows:

$$ZnAl-CO_3^{2-}-HT+2Cl^-\rightarrow ZnAl-2Cl^--HT+CO_3^{2-} \quad (5)$$

Based on the ion exchange process, the release of CO_3^{2-} anions concentrated on the coating surface led to the formation of a diffusion boundary layer containing high concentrations of CO_3^{2-} ions. Using the competitive adsorption, the diffusion boundary layer containing CO_3^{2-} ions impairs the adsorption of Cl^- on the surface of the HT conversion films which could effectively improve the pitting resistance property of the EG steel surface.

Besides, the anodic dissolution of the zinc coating can lead to the pH change and ion contents in the local solution near the Zn surface [50]. The structure of ZnAl-HT crystals of the conversion layer may be partially destroyed in this situation, releasing Zn^{2+} and Al^{3+} cations (Fig. 13) [44]. The ZnO recrystallization of the Zn^{2+} ions released due to corrosion of the Zn surface, where a high concentration of Zn^{2+} ions exist, can lead to the sealing of the damaged ZnAl-HT conversion films while retaining the chloride entrapment properties of the HT layer.

4. Conclusions

The ZnAl-CO_3^{2-} HT conversion films were successfully synthetized on EG steel substrate with various Al^{3+}/Zn^{2+} ratios by the “in situ” growth method at pH 12 and room temperature. It was shown that the Al^{3+}/Zn^{2+} ratio affected the morphology, structure, thickness, and protective properties of the ZnAl-HT conversion films. The polarization curves indicated the ZnAl-HT conversion films act as anodic inhibitive species. The layer is still detected after an exposure period of 24 h in 0.1 M NaCl solution. Nevertheless, the corrosion resistance of HT 5/1, HT 5/2, and HT 5/3 films decreased significantly. In contrast, the anti-corrosion of HT 5/4 and HT 5/5 remained stable during immersion time. The protection performance of the ZnAl-HT films can be ascribed to the barrier function, the ion-exchange competitive adsorption for chloride ions, and the protective deposition of ZnO which seals the hydrotalcite structure on EG steel surface.

CRediT authorship contribution statement

Thu Thuy Pham: Investigation, Methodology, Validation, Writing – original draft. **Thuy Duong Nguyen:** Investigation, Validation, Formal analysis. **Anh Son Nguyen:** Investigation, Validation. **Yoann Paint:** Investigation, Validation. **Maurice Gonon:** Investigation, Validation. **Thi Xuan Hang To:** Writing – review & editing, Supervision, Methodology, Validation. **Marie-Georges Olivier:** Writing – review & editing, Supervision, Funding acquisition.

Declaration of competing interest

The Université of Mons has received a financial funding coming from the ARES (Belgium) in the framework of the PRD Project "RENFORCEMENT DE L'EXPERTISE ENVIRONNEMENTALE DU CENTRE DE COMPÉTENCES EN PROTECTION CONTRE LA CORROSION ET EN ÉLECTROCHIMIE", Institute of Tropical Technology, Vietnam, 2020–2025.

This project attributed a PhD grant to Pham Thu Thuy for coming in Belgium for a part of her research (six months per year).

Acknowledgments

The authors gratefully acknowledge the financial support of the Vietnam Academy of Science and Technology for young researchers, the Académie de Recherche et d'Enseignement Supérieur (ARES Belgium) through the Development Cooperation project between Vietnam and Belgium (PRD 2020-2025: Renforcement de l'expertise environnementale du centre de compétences en protection contre la corrosion et en électrochimie), and Sebastien Colmant from the Metallurgy Department (UMONS) for his help to prepare the embedded samples.

References

[1] A. Algahtani, Fiber yttrium aluminum garnet laser cladding of mild steel with SiC and Al2O3 powders, Sci. Adv. Mater. 11 (2019) 979–985.
[2] N.A. Negm, N.G. Kandile, E.A. Badr, M.A. Mohammed, Gravimetric and electrochemical evaluation of environmentally friendly nonionic corrosion inhibitors for carbon steel in 1 M HCl, Corros. Sci. 65 (2012) 94–103.
[3] J. Rodriguez, L. Chenoy, A. Roobroeck, S. Godet, M.G. Olivier, Effect of the electrolyte pH on the corrosion mechanisms of Zn-Mg coated steel, Corros. Sci. 108 (2016) 47–59.
[4] X.G. Zhang, Corrosion and electrochemistry of zinc, Springer Science & Business Media, 1996.
[5] Z. Gao, D. Zhang, X. Li, S. Jiang, Q. Zhang, Current status, opportunities and challenges in chemical conversion coatings for zinc, colloids surfA 546 (2018) 221–236.
[6] R. Buchheit, H. Guan, Formation and characteristics of Al-Zn hydrotalcite coatings on galvanized steel, J. Coat. Technol. Res. 1 (2004) 277–290.
[7] K. Hoshino, S. Furuya, R.G. Buchheit, Effect of NO3− intercalation on corrosion resistance of conversion coated zn-Al-CO3 LDHs on electrogalvanized steel, J. Electrochem. Soc. 165 (2018) C461–C468.
[8] K. Hoshino, S. Furuya, R.G. Buchheit, Effect of solution pH on layered double hydroxide formation on electrogalvanized steel sheets, J. Mater. Eng. Perform. 28 (2019) 2237–2244.
[9] S.-H. Zhang, G. Kong, J.-T. Lu, C.-S. Che, L.-Y. Liu, Growth behavior of lanthanum conversion coating on hot-dip galvanized steel, Surf. Coat. Technol. 259 (2014) 654–659.
[10] X. Bai, T.H. Tran, D. Yu, A. Vimalanandan, X. Hu, M. Rohwerder, Novel conducting polymer based composite coatings for corrosion protection of zinc, Corros. Sci. 95 (2015) 110–116.
[11] A. Pruna, L. Pilan, Electrochemical study on new polymer composite for zinc corrosion protection, Compos. Part B 43 (2012) 3251–3257.
[12] M. Poelman, M. Fedel, C. Motte, D. Lahem, T. Urios, Y. Paint, F. Deflorian, M. G. Olivier, Influence of formulation and application parameters on the performances of a sol–gel/clay nanocomposite on the corrosion resistance of hot-dip galvanized steel. Part I. Study of the sol preparation parameters, Surf. Coat. Technol. 274 (2015) 1–8.
[13] M. Pantoja, J. Abenojar, M. Martínez, F. Velasco, Silane pretreatment of electrogalvanized steels: effect on adhesive properties, Int. J. Adhes. Adhes. 65 (2016) 54–62.
[14] V. Shkirskiy, P. Keil, H. Hintze-Bruening, F. Leroux, P. Vialat, G. Lefèvre, K. Ogle, P. Volovitch, Interfaces, factors affecting MoO42– inhibitor release from Zn2Al based layered double hydroxide and their implication in protecting hot dip galvanized steel by means of organic coatings, ACS Appl. Mater. Interfaces 7 (2015) 25180–25192.
[15] W. Feitknecht, M. Gerber, Zur kenntnis der doppelhydroxyde und basischen doppelsalze III. Über magnesium-aluminiumdoppelhydroxyd, Helv. Chim. Acta 25 (1942) 131–137.
[16] S.J. Mills, A.G. Christy, R.T. Schmitt, The creation of neotypes for hydrotalcite, Mineral. Mag. 80 (2016) 1023–1029.
[17] Y. Tang, F. Wu, L. Fang, T. Guan, J. Hu, S. Zhang, A comparative study and optimization of corrosion resistance of ZnAl layered double hydroxides films intercalated with different anions on AZ31 mg alloys, Surf. Coat. Technol. 358 (2019) 594–603.
[18] C. Jing, B. Dong, A. Raza, T. Zhang, Y. Zhang, Corrosion inhibition of layered double hydroxides for metal-based systems, NanoMater. Sci. 3 (2021) 47–67.
[19] D.T. Nguyen, H.T.X. To, J. Gervasi, Y. Paint, M. Gonon, M.-G. Olivier, Corrosion inhibition of carbon steel by hydrotalcites modified with different organic carboxylic acids for organic coatings, Prog. Org. Coat. 124 (2018) 256–266.
[20] T.D. Nguyen, A.S. Nguyen, B.A. Tran, K.O. Vu, D.L. Tran, T.T. Phan, N. Scharnagl, M.L. Zheludkevich, T.X.H. To, Molybdate intercalated hydrotalcite/graphene oxide composite as corrosion inhibitor for carbon steel, Surf. Coat. Technol. 399 (2020), 126165.
[21] J. Rodriguez, E. Bollen, T.D. Nguyen, A. Portier, Y. Paint, M.G. Olivier, Incorporation of layered double hydroxides modified with benzotriazole into an epoxy resin for the corrosion protection of Zn-Mg coated steel, Prog. Org. Coat. 149 (2020) 1058942.
[22] Y. Song, Y. Tang, L. Fang, F. Wu, X. Zeng, J. Hu, S.F. Zhang, B. Jiang, H. Luo, Enhancement of corrosion resistance of AZ31 mg alloys by one-step in situ synthesis of ZnAl-LDH films intercalated with organic anions (ASP, La), J. Magnes. Alloy 9 (2021) 658–667.
[23] J. Lin, C. Hsia, J. Uan, Characterization of Mg, Al-hydrotalcite conversion film on mg alloy and Cl− and CO32- anion-exchangeability of the film in a corrosive environment, Scr. Mater. 56 (2007) 927–930.
[24] J. Lin, J. Uan, Formation of mg, Al-hydrotalcite conversion coating on mg alloy in aqueous HCO3−/CO32− and corresponding protection against corrosion by the coating, Corros. Sci. 51 (2009) 1181–1188.
[25] B.-L. Yu, J.-K. Lin, J.-Y. Uan, Applications of carbonic acid solution for developing conversion coatings on mg alloy, Trans. Nonferrous Met. Soc. China 20 (2010) 1331–1339.
[26] F. Zhang, C.-L. Zhang, L. Song, R.-C. Zeng, Z.-G. Liu, H.-Z. Cui, Corrosion of in-situ grown MgAl-LDH coating on aluminum alloy, Trans. Nonferrous Met. Soc. China 25 (2015) 3498–3504.
[27] A. Mikhailau, H. Maltanava, S.K. Poznyak, A.N. Salak, M.L. Zheludkevich, K. A. Yasakau, M.G.S. Ferreira, One-step synthesis and growth mechanism of nitrate intercalated ZnAl LDH conversion coatings on zinc, Chem. Commun. 55 (2019) 6878–6881.
[28] A.C. Bouali, M.H. Iuzviuk, M. Serdechnova, K.A. Yasakau, D.C.F. Wieland, G. Dovzhenko, H. Maltanava, I.A. Zobkalo, M.G.S. Ferreira, M.L. Zheludkevich, Zn-Al LDH growth on AA2024 and zinc and their intercalation with chloride: comparison of crystal structure and kinetics, Appl. Surf. Sci. 501 (2020), 144027.
[29] N. Palapa, T. Taher, P. Siregar, N. Normah, N. Juleanti, A. Wijaya, A. Badri, A. Lesbani, High structural stability and adsorption capacity of Zn/Al-biochar and Cu/Al-biochar toward adsorption of Cr(VI), J. Ecol. Eng. 22 (2021) 213–223.
[30] Y. Yang, X. Yan, X. Hu, R. Feng, M. Zhou, In-situ growth of ZIF-8 on layered double hydroxide: effect of Zn/Al molar ratios on their structural, morphological and adsorption properties, J. Colloid Interface Sci. 505 (2017) 206–212.
[31] B. Zhou, X. Wei, Y. Wang, Q. Huang, B. Hong, Y. Wei, Effect of lanthanum addition on microstructures and corrosion behavior of ZnAl-LDHs film of 6061 aluminum alloys, Surf. Coat. Technol. 379 (2019) 1250562.
[32] V.Z. Asl, J. Zhao, M.J. Anjum, S. Wei, W. Wang, Z. Zhao, The effect of cerium cation on the microstructure and anti-corrosion performance of LDH conversion coatings on AZ31 magnesium alloy, J. Alloys Compd. 821 (2020), 153248.
[33] A.A.A. Ahmed, Z.A. Talib, M.Z. bin Hussein, A. Zakaria, Zn–Al layered double hydroxide prepared at different molar ratios: preparation, characterization, optical and dielectric properties, J. Solid State Chem. 191 (2012) 271–278.
[34] R. Comparelli, E. Fanizza, M. Curri, P. Cozzoli, G. Mascolo, A. Agostiano, UV-induced photocatalytic degradation of azo dyes by organic-capped ZnO nanocrystals immobilized onto substrates, Appl. Catal. B 60 (2005) 1–11.
[35] S. Mallakpour, M. Hatami, C.M. Hussain, Recent innovations in functionalized layered double hydroxides: fabrication, characterization, and industrial applications, Adv. Colloid Interf. Sci. 283 (2020), 102216.
[36] E. Kanezaki, Thermal behavior of the hydrotalcite-like layered structure of mg and Al-layered double hydroxides with interlayer carbonate by means of in situ powder HTXRD and DTA/TG, Solid State Ionics 106 (1998) 279–284.
[37] T. Ishikawa, K. Matsumoto, K. Kandori, T. Nakayama, Synthesis of layered zinc hydroxide chlorides in the presence of Al(III), J. Solid State Chem. 179 (2006) 1110–1118.
[38] A.A.A. Ahmed, Z.A. Talib, M.Z. Hussein, Influence of metallic molar ratio on the electron spin resonance and thermal diffusivity of Zn–Al layered double hydroxide, J. Nanomater. 2013 (2013) 1–9.
[39] K. Dutta, S. Das, A. Pramanik, Concomitant synthesis of highly crystalline Zn-Al layered double hydroxide and ZnO: phase interconversion and enhanced photocatalytic activity, J. Colloid Interface Sci. 366 (2012) 28–36.
[40] Y. Meng, L. Liu, D. Zhang, C. Dong, Y. Yan, A.A. Volinsky, L.N. Wang, Initial formation of corrosion products on pure zinc in saline solution, Bioact. Mater. 4 (2019) 87–96.
[41] H. He, H. Kang, S. Ma, Y. Bai, X. Yang, High adsorption selectivity of ZnAl layered double hydroxides and the calcined materials toward phosphate, J. Colloid Interface Sci. 343 (2010) 225–231.
[42] N. Iyi, T. Sasaki, Deintercalation of carbonate ions and anion exchange of an Al-rich MgAl-LDH (layered double hydroxide), Appl. Clay Sci. 42 (2008) 246–251.

[43] C. Gomes, Z. Mir, R. Sampaio, A. Bastos, J. Tedim, F. Maia, C. Rocha, M. Ferreira, Use of ZnAl-layered double hydroxide (LDH) to extend the service life of reinforced concrete, Materials (Basel) 13 (2020) 1769.
[44] T. Yan, S. Xu, Q. Peng, L. Zhao, X. Zhao, X. Lei, F. Zhang, Self-healing of layered double hydroxide film by dissolution/recrystallization for corrosion protection of aluminum, J. Electrochem. Soc. 160 (2013) C480.
[45] K. Kamburova, N. Boshkova, N. Boshkov, T. Radeva, Composite coatings with polymeric modified ZnO nanoparticles and nanocontainers with inhibitor for corrosion protection of low carbon steel, Colloids Surf. A Physicochem. Eng. Asp. 609 (2021), 125741.
[46] M. Arenas, D. Damborenea, Use of electrochemical impedance spectroscopy to study corrosion of galvanised steel in 0·6M NaCl solution, Corros. Eng. Sci. Technol. 41 (2006) 228–234.
[47] J.L. Matos, V. Cerveira, S.M. Manhabosco, S.P.G. Valenzuela, D.P. Dick, L.F. P. Dick, Humic acid: a new corrosion inhibitor of zinc in chlorides, Electrochim. Acta 397 (2021).
[48] F. Zhang, Z.-G. Liu, R.-C. Zeng, S.-Q. Li, H.-Z. Cui, L. Song, E.-H. Han, Corrosion resistance of Mg–Al-LDH coating on magnesium alloy AZ31, Surf. Coat. Technol. 258 (2014) 1152–1158.
[49] R.-C. Zeng, X.-T. Li, Z.-G. Liu, F. Zhang, S.-Q. Li, H.-Z. Cui, Corrosion resistance of Zn–Al layered double hydroxide/poly (lactic acid) composite coating on magnesium alloy AZ31, FrontMater. Sci. 9 (2015) 355–365.
[50] E. Tada, K. Sugawara, H. Kaneko, Distribution of pH during galvanic corrosion of a Zn/steel couple, Electrochim. Acta 49 (2004) 1019–1026.